Electronic Supplementary Information (ESI)

Atomic-Layer-Deposited Ultrathin Co_9S_8 on Carbon Nanotubes: an Efficient Bifunctional Electrocatalyst for Oxygen Evolution/Reduction Reactions and Rechargeable Zn-Air Batteries

*Hao Li, Zheng Guo, and Xinwei Wang**

School of Advanced Materials, Shenzhen Graduate School, Peking University, Shenzhen 518055, China
E-mail: wangxw@pkusz.edu.cn

Table S1. Comparison of the *d*-spacings measured by TEM (Figure 1g) with the reference data for the face-centered cubic Co_9S_8 structure (JCPDS 86-2273). The TEM results were also consistent with our previously reported data (Li et al. *Nano Lett.* 2015, **15**, 6689).

JCPDS 86-2273		**TEM results**
(h k l)	***d* (Å)**	**Measured *d* (Å)**
(2 2 0)	**3.5083**	**3.52**
(2 2 2)	**2.8645**	**2.84**
(4 0 0)	**2.4808**	**2.50**
(4 2 0)	**2.2188**	**2.24**
(4 4 0)	**1.7542**	**1.76**

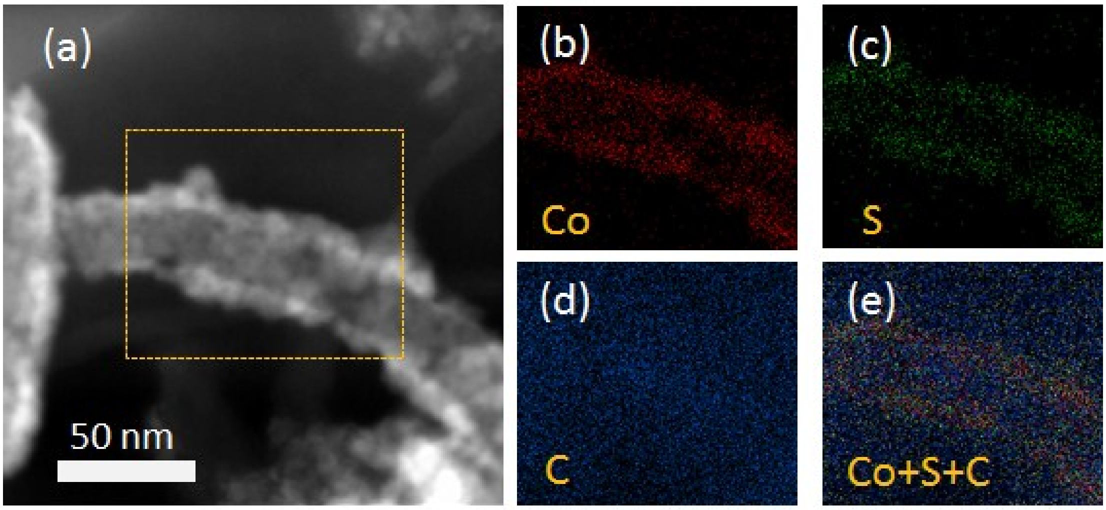

Figure S2. (a) STEM image of the ALD Co_9S_8/CNT sample, and the corresponding elemental maps of (b) Co, (c) S, (d) C, and (e) their overlay.

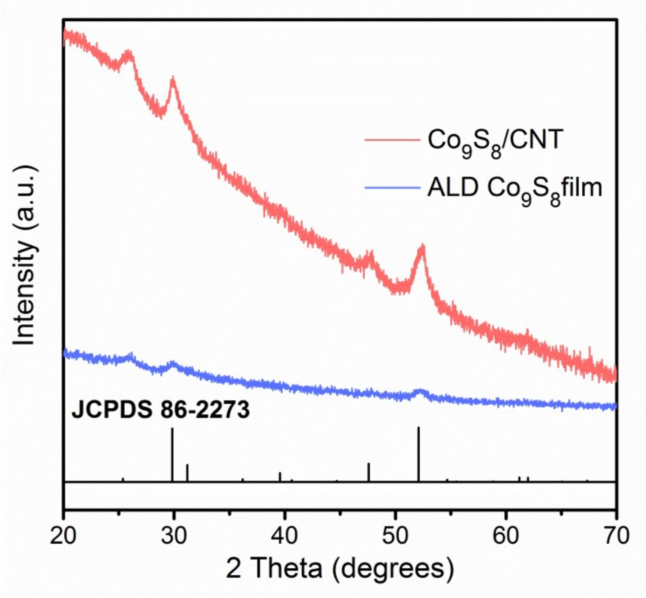

Figure S3. XRD patterns for the ALD Co_9S_8/CNT and ALD Co_9S_8 thin film.

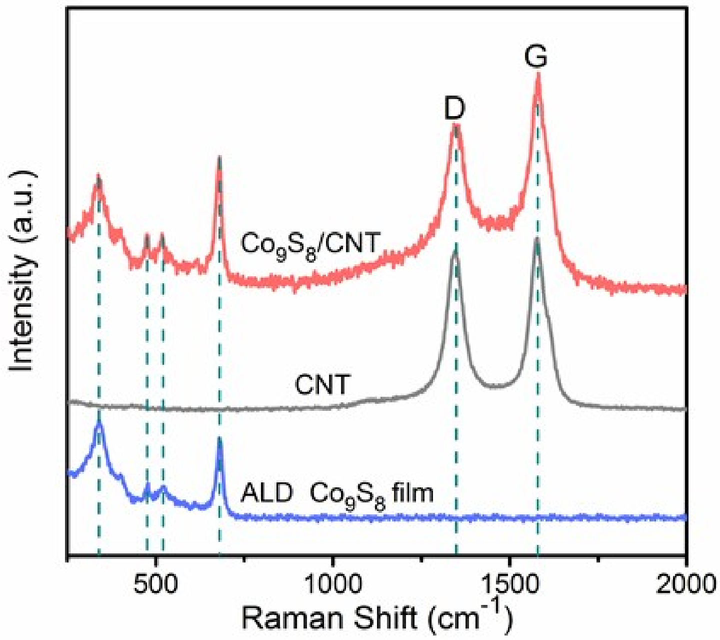

Figure S4. Raman spetra for the ALD Co_9S_8/CNT, uncoated bare CNTs, and ALD Co_9S_8 thin film.

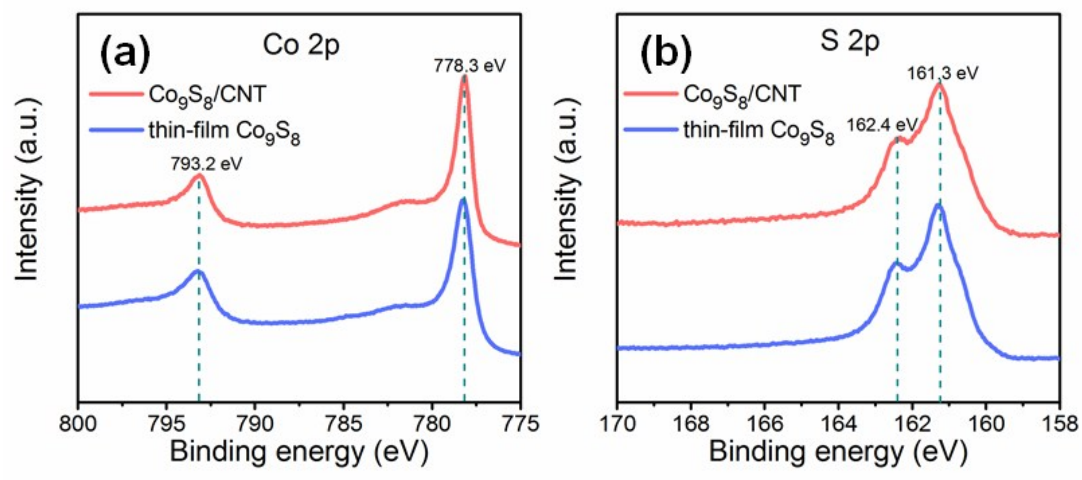

Figure S5. Comparison of the XPS spectra of (a) Co 2p and (b) S 2p peaks for the ALD Co_9S_8/CNT and ALD Co_9S_8 thin film.

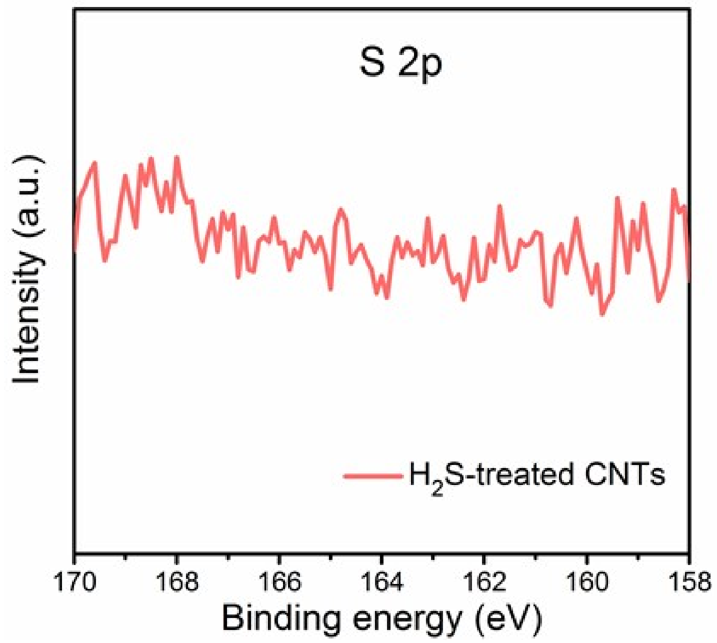

Figure S6. XPS S 2p spectrum of H_2S-treated CNTs. The H_2S treatment was performed following the same deposition conditions as for the ALD of Co_9S_8 on CNTs except that no Co precursor was dosed (i.e. only dosing H_2S).

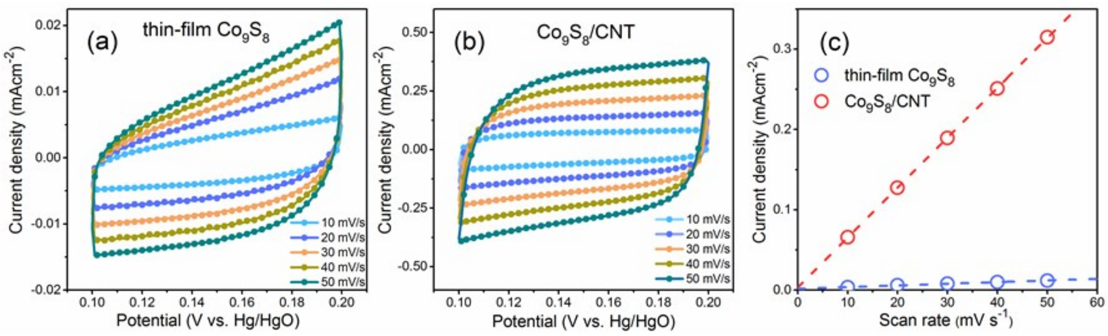

Figure S7. CV scans for the ALD-prepared (a) thin-film Co_9S_8 and (b) Co_9S_8/CNT electrocatalysts. The scans were performed in the non-Faradic region of 0.1 to 0.2 V (vs. Hg/HgO) with the scan rate varied as 10, 20, 30, 40, and 50 mV/s. (c) Plot of the current density versus scan rate for both of the catalysts, from which the double layer capacitances can be extracted from the slopes of the linear fits, respectively. The extracted double layer capacitances were 6.22 and 0.205 mF/cm^2 for the Co_9S_8/CNT and thin-film Co_9S_8 catalysts, respectively. The former was 30 times larger than the latter.

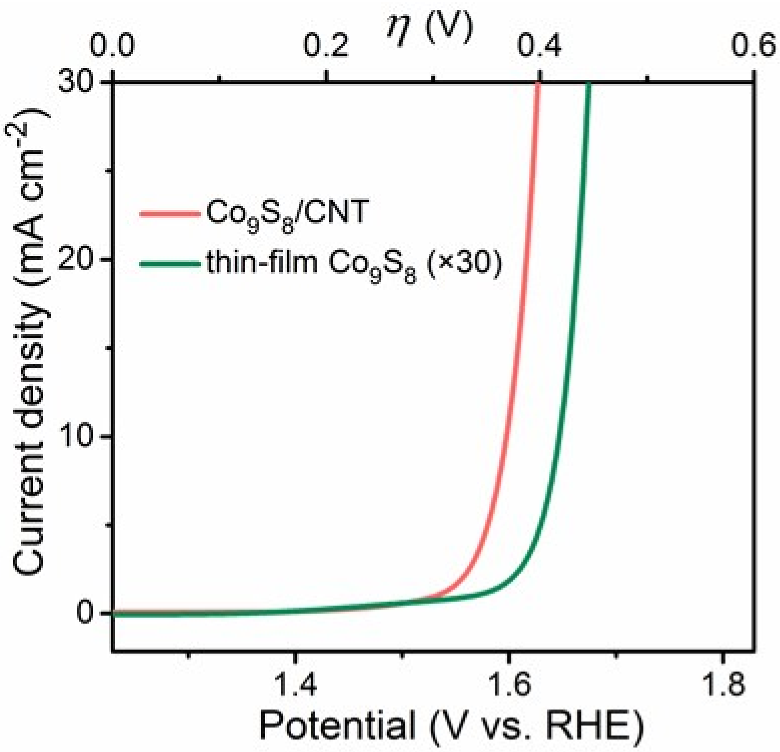

Figure S8. To take into account the effect of enlarged surface area for the Co_9S_8/CNT, the curve for the thin-film Co_9S_8 shown in Figure 2a is replotted herein by multiplying the current density by 30. The multiplied current density of the thin-film Co_9S_8 was still inferior to that of the Co_9S_8/CNT, suggesting that some other effects, perhaps from the CNT support, might additionally contribute to the enhanced OER performance of the Co_9S_8/CNT.

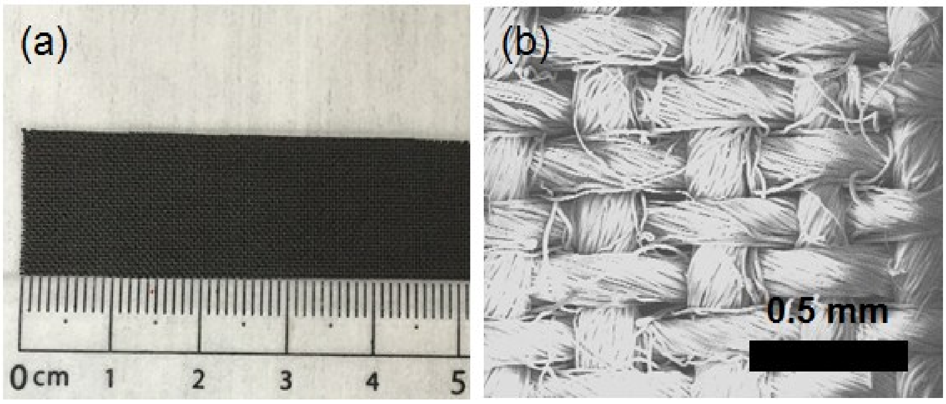

Figure S9. (a) Photograph and (b) SEM image of a piece of carbon cloth.

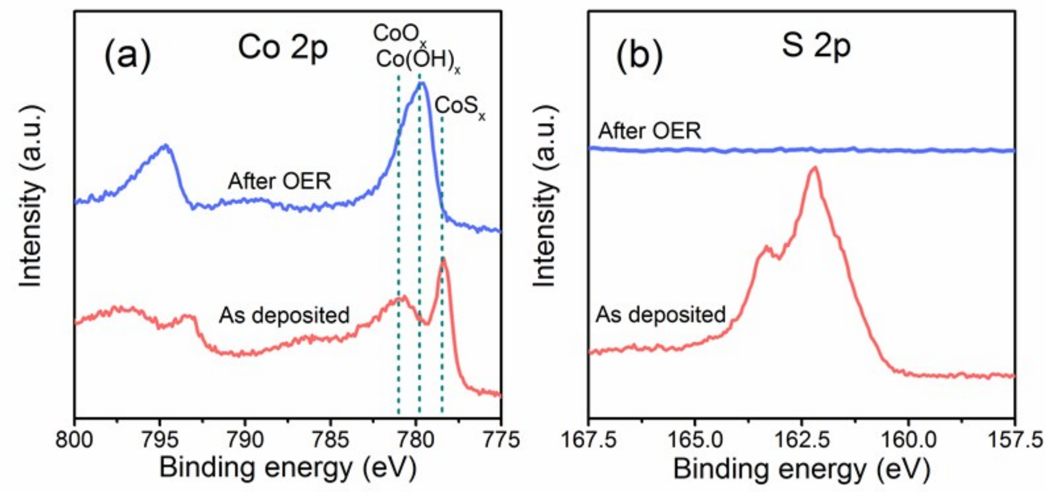

Figure S10. Comparison of the (a) Co 2p and (b) S 2p XPS spectra for the Co_9S_8/CNT catalyst as prepared and after OER.

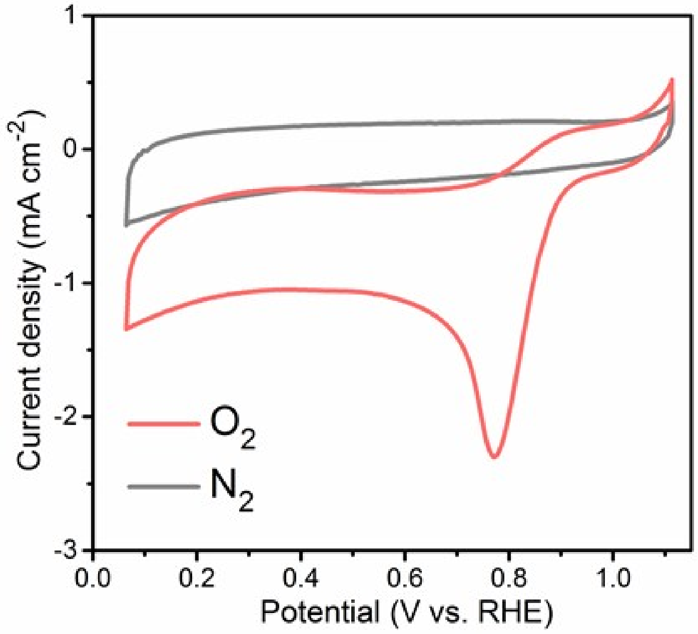

Figure S11. CV curves for the Co_9S_8/CNT electrocatalyst measured in O_2- and N_2-saturated 0.1 mol/L KOH, respectively. The scan rate was 100 mV/s.

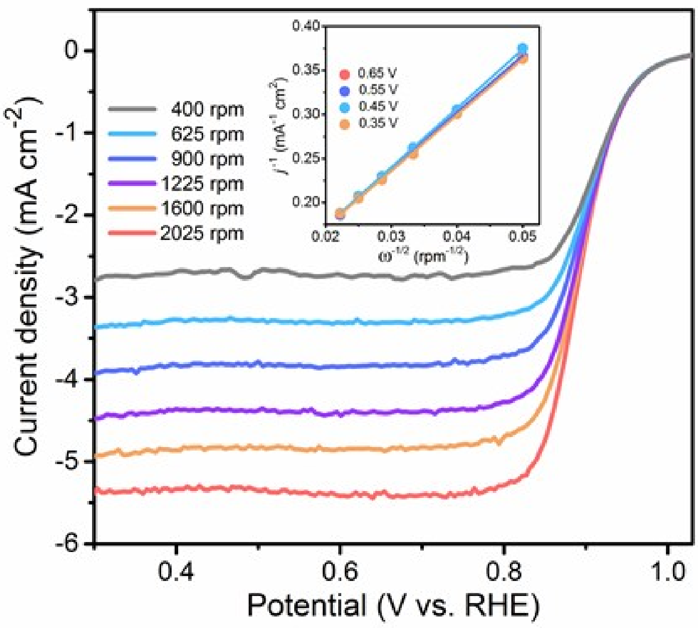

Figure S12. RDE voltammograms of the Pt/C catalyst with various rotation speeds for the electrode. The electrolyte was O_2-saturated 0.1 mol/L KOH, and the voltage scan rate was 10 mV/s. The inset shows the corresponding Koutecky-Levich plots (j^{-1} vs. $\omega^{-1/2}$).

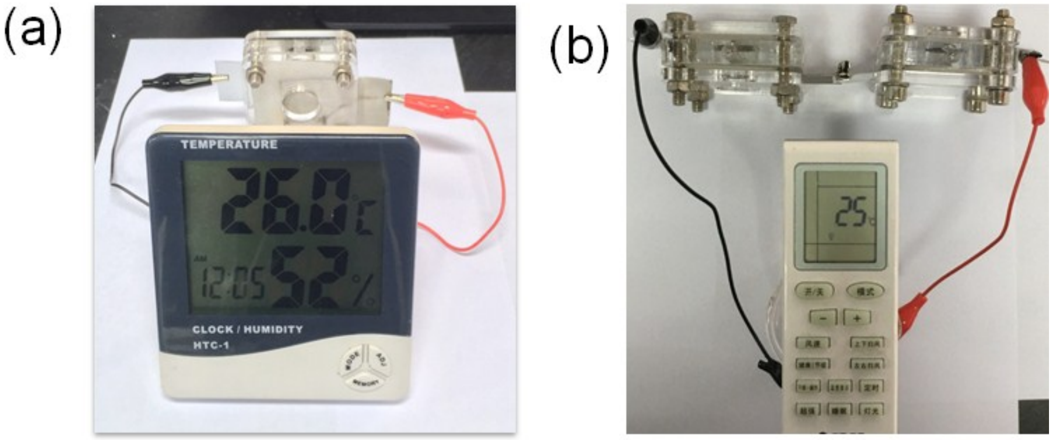

Figure S13. Photographs showing that the ALD-Co_9S_8/CNT-based aqueous Zn-air batteries can be used in replacement of (a) a 1.5 V coin cell to power a temperature/humidity monitor and (b) two AAA batteries to power a remote controller, respectively.

Figure S14. Photograph of a solid-state rechargeable Zn-air battery using the ALD Co_9S_8/CNT catalyst for the air electrode. The open-circuit voltage was measured as 1.290 V.

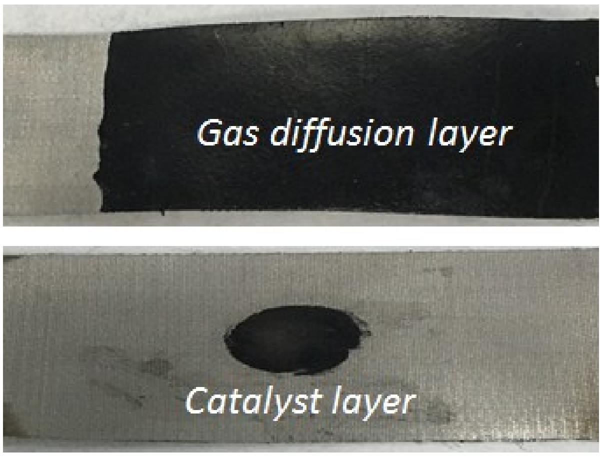

Figure S15. Photographs of an air cathode for the aqueous Zn-air battery. The cathode had a gas diffusion layer (upper) on one side of its stainless steel mesh, and the catalyst was loaded on the other side (lower).

Table S2. Comparison of OER performance with various reported non-precious catalysts.

Catalyst	η (V)	Tafel slope	Reference
Co_9S_8/CNT/CC	**0.321**	**58**	**This work**
Co_9S_8/CNT	**0.369**	**58**	**This work**
N-Co_9S_8/graphene	0.409	82.7	*Energy Environ. Sci.* 2016, 9, 1320
CoS_2/N,S-GO	0.381	75	*ACS Catal.* 2015, 5, 3625
Co_3S_4 nanosheets	0.363	90	*Angew. Chem.* 2015, 127, 11383
Co_9S_8/MoS_2/carbon nanofiber	0.43	61	*Adv. Mater.* 2015, 27, 4752
$NiCo_2S_4$/graphene	0.47	-	*ACS Appl. Mater. Interfaces* 2013, 5, 5002
Co_3O_4/Au	0.39	60	*Adv. Mater.* 2014, 26, 3950
Co/Co_3O_4/N-CNT	0.421	91.5	*Angew. Chem. Int. Ed.* 2016, 55, 4087
$ZnCo_2O_4$/N-CNT	0.421	70.6	*Adv. Mater.* 2016, 28, 3777
$Co_{50}Zn_{50}$/nanoporous carbon	0.44-0.48	86-92	*Energy Environ. Sci.* 2016, 9, 1661
N,S-porous carbon	0.46	292	*Energy Environ. Sci.* 2017, 10, 742
P-g-C_3N_4/carbon fiber paper	0.401	61.6	*Angew. Chem. Int. Ed.* 2015, 54, 4646

Table S3. Comparison of ORR performance with various reported non-precious catalysts.

Catalyst	E_{onset} (V) vs. RHE	$E_{1/2}$ (V) vs. RHE	n	Reference
Co_9S_8/CNT	**0.94**	**0.82**	**3.84-3.90**	**This work**
N-Co_9S_8/graphene	0.941	0.74	3.7-3.9	*Energy Environ. Sci.* 2016, 9, 1320
$Co_{1-x}S$/graphene	0.87	-	~4	*Angew. Chem. Int. Ed.* 2011, 50, 10969
Co_9S_8/N,S-porous-CNT	-	0.79	3.94	*NPG Asia Mater.* 2016, 8, e308
CoS_2-CNT/graphene	0.78	-	-	*J. Mater. Chem. A* 2016, 3, 6340
Co_9S_8/N-carbon	0.91	-	3.63-3.88	*Electrochim. Acta* 2016, 191, 776
CoS_x/N,S-graphene	0.82	-	3.5-3.55	*RSC Adv.* 2015, 5, 7280
CoP nanocrystals	0.80	0.70	3.5	*Nano Lett.* 2015, 15, 7616
CoO/N-CNT	0.93	-	3.9	*J. Am. Chem. Soc.* 2012, 134, 15849
Co/Co_3O_4/N-CNT	-	0.80	3.78	*Angew. Chem. Int. Ed.* 2016, 55, 4087
$ZnCo_2O_4$/N-CNT	0.95	0.87	3.8	*Adv. Mater.* 2016, 28, 3777
$Ba_{0.5}Sr_{0.5}Co_{0.8}Fe_{0.2}O_{3-\delta}$/acetylene black	0.84	-	3.43	*ACS Catal.* 2014, 4, 1061
Fe_3O_4/N-graphene	0.86	-	3.72-3.95	*J. Am. Chem. Soc.* 2012, 134, 9082
P-g-C_3N_4/carbon fiber paper	0.94	0.67	4	*Angew. Chem. Int. Ed.* 2015, 54, 4646